2018 International Symposium on Nonlinear Theory and Its Applications,
NOLTA2018, Tarragona, Spain, September 2-6, 2018

Bifurcation analysis of a model of cardiovascular variability

Franco S. Gentile†⋆, Griselda R. Itovich∗, Guillermo L. Calandrini†⋆‡ and Jorge L. Moiola⋆‡

†Departamento de Matemática, Universidad Nacional del Sur, B8000CPB Bahía Blanca, Argentina
⋆ Instituto de Investigaciones en Ingeniería Eléctrica - IIIE (UNS-CONICET), B8000CPB Bahía Blanca, Argentina
∗ Escuela de Producción, Tecnología y Medio Ambiente, Sede Alto Valle, Universidad Nacional de Río Negro, R8336ATG Villa Regina, Argentina
‡Dpto. de Ingeniería Eléctrica y Computadoras, Universidad Nacional del Sur, B8000CPB Bahía Blanca, Argentina

Abstract—In this article, a model of hearth rate variability including baroreflex control is studied analytically using a frequency-domain approach. Baroreflex is a feedback control mechanism with an inherent time-delay, which can cause oscillations via Hopf bifurcation. Some local results on the nonlinear behavior of the system, as well as approximations of the periodic solutions, are obtained.

1. Introduction

It is well known that modeling and analyzing the cardiovascular system (CS) is a challenging task, and several approaches exist in the literature. An excellent overview on the most relevant works in this field can be seen in [1].

Among the different viewpoints to study the CS, one approach considers the modeling via delay-differential equations (DDE). Following this idea, Cavalcanti & Belardinelli [2] and Ottesen [3] studied the effect of time-delay in relation with baroreflex control, and they found that it can cause the appearance of oscillations and even chaos in the CS.

Since then, several authors considered DDE-based models to study the CS. Recently, the stability margin based on the Lyapunov theory was computed in a DDE model in [4], where the variation of several parameters was considered. In [5], an enhanced model with multiple delays was proposed and its stability was investigated.

In this work, the original model introduced in [2] is considered. As the system is naturally a feedback one, its study through the frequency-domain approach proposed in [6, 7] is straightforward. Using this technique, analytical conditions for the appearance of Hopf bifurcation are derived. Moreover, approximate solutions of the emerging periodic orbits are constructed. Finally, Hopf bifurcation curves in two-parameter spaces are also given.

2. The model

Cavalcanti & Belardinelli's model [2] was proposed to study the baroreflex characteristic effect on cardiovascular variability.

The blood circulation is described by an analogous electrical circuit, called Windkessel model [8]. The blood flow is analogous to the electrical current, and blood pressure

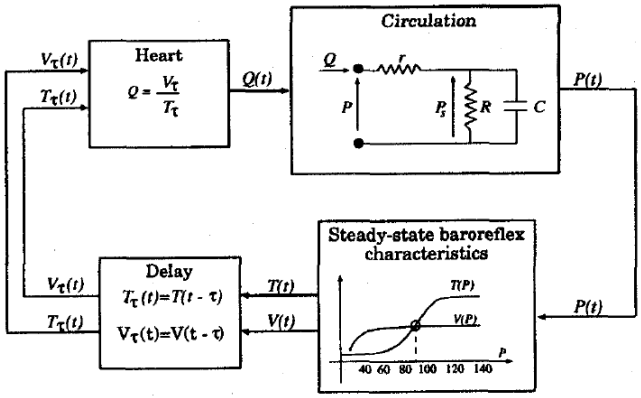

Figure 1: Schematic representation of the system under study, taken from [2].

is analogous to the voltage at the input of the circuit. It is described by the equations

$$\begin{aligned} \frac{dP_s(t)}{dt} &= w_t\,[RQ(t) - P_s(t)]\,, \quad w_t = \frac{1}{RC} \\ P(t) &= P_s(t) + rQ(t), \end{aligned} \tag{1}$$

where $P(t)$ is the mean aortic pressure, $Q(t)$ is the mean aortic blood flow and $P_s(t)$ is an intermediate voltage in the circuit. R represents the peripheral resistance, which refers to the flow resistance encountered by the blood as it flows through the systemic arterial. The capacity C is the arterial compliance, and it refers to the elasticity and extensibility of the major artery. Finally, r represents the resistance to blood flow due to the aortic valve. In this way, $P - P_s$ is the pressure drop produced by the aortic valve.

The considered model is non-pulsatile, which means that $Q(t)$ is simply the ratio between the stroke volume, $V(t)$, and the cardiac period, $T(t)$. It follows that:

$$Q(t) = \frac{V(t-\tau)}{T(t-\tau)}, \tag{2}$$

where τ is the delay of baroreflex control, which senses the aortic pressure and adjusts both heart rate and stroke volume. Such an adjustment is modeled using the functions:

$$\begin{aligned} T(P) &= T_s + \frac{T_m - T_s}{1 + \gamma e^{-\alpha P/P_n}}, \quad \gamma >> T_m - T_s, \\ V(P) &= \frac{V_{max}}{1 + \beta\,(P/P_v - 1)^{-k}}, \quad P \geq P_v, \end{aligned} \tag{3}$$

where $T(P)$ reproduces the characteristic saturation effects in heart rate when pressure reaches low and high levels. The lower (T_s) and upper (T_m) levels establish the shorter and longer cardiac period and match, respectively, the maximal vasodepressor-induced sympathetic excitation and the maximum pressor-induced vagal activation. P_n corresponds to the steady level of mean arterial pressure; α and γ, determine range and slope of the linear region of the mean pressure-heart period curve. On the other hand, $V(P)$ models the steady-state stroke volume-pressure relationship, where V_{max} is the maximum stroke volume and P_v is the pressure for which cardiac output is null.

The values of parameters involved in (1) and (3) are listed in Table 1, which are fixed in first instance. The only bifurcation parameter is the delay τ.

Table 1: Parameter values.

Windkessel		
R	$1.2\ 10^3$	$\left[dyn\ s/cm^5\right]$
r	52	$\left[dyn\ s/cm^5\right]$
C	$1\ 10^{-3}$	$\left[cm^5/dyn\right]$
Heart Rate		
T_s	0.66	$[s]$
T_m	1.2	$[s]$
P_n	89	$[mmHg]$
α	31	
γ	$6.7\ 10^{13}$	
Stroke Volume		
V_{max}	86	$\left[cm^3\right]$
P_v	25	$[mmHg]$
β	72	
k	7	

Equations (1), (2) and (3) define completely the model under study, which is shown schematically in Fig. 1.

3. Frequency-domain analysis

Model (1)-(2)-(3) is a feedback system. For the linear Windkessel subsystem, by considering the Laplace transforms of $P(t)$ and $Q(t)$ and from (1), it follows that

$$\frac{\mathcal{L}\{P\}}{\mathcal{L}\{Q\}} \triangleq G(s) = a\,\frac{rs + w_t(R+r)}{s + w_t}. \tag{4}$$

Note that $G(s)$ is simply the complex impedance of the electrical circuit shown in Fig. 1. The input of the linear block is $Q(t)$ and the output is $P(t)$. The constant a is included only for units conversion, since P_s is given in $\left[dyn/cm^2\right]$ and P is given in $[mmHg]$, thus $P = a(P_s + rQ)$ and it follows that $a = 7.5006\ 10^{-4}$.

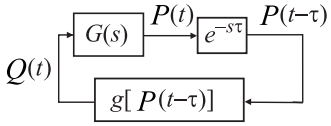

Figure 2: Block representation for the frequency-domain analysis.

The two nonlinear functions describing the hearth period and stroke volume in (3) can be combined into a single nonlinearity by defining

$$g\,(P_\tau) = \frac{V(P_\tau)}{T(P_\tau)}, \tag{5}$$

where $P_\tau = P(t-\tau)$. The delay dynamics can be considered to affect the output of the linear block, thus completing the frequency-domain model shown in Fig. 2. The transfer function for the linear part is

$$G^*(s) = a\,\frac{rs + w_t(R+r)}{s + w_t}\,e^{-s\tau}. \tag{6}$$

The possible equilibrium points are given by $g(P^*)G^*(0) = P^*$, that is

$$\frac{V(P^*)}{T(P^*)}a(r+R) = P^*. \tag{7}$$

The above equation can be solved graphically, intersecting the curve of $g(P)$ with the straight line $\frac{1}{a(r+R)}P$, as shown in Fig. 3. There are two equilibrium points, $P_1^* = 73.9642$ and $P_2^* = 89.0408$. Consider the following expressions for the linear variational analysis:

$$J_1 \triangleq \frac{dg}{dP}\Big|_{P=P_1^*} = 4.3896, \quad J_2 \triangleq \frac{dg}{dP}\Big|_{P=P_2^*} = -3.6487, \tag{8}$$

then proceed to the stability analysis. The closed-loop transfer function for the linearized system is

$$H(s) = \frac{G^*(s)}{1 - G^*(s)J_k}, \quad k = 1, 2, \tag{9}$$

then it follows that the critical stability condition is $G^*(i\omega_0)J_k = 1$, or equivalently, $G^*(i\omega_0) = 1/J_k$. Figure 4

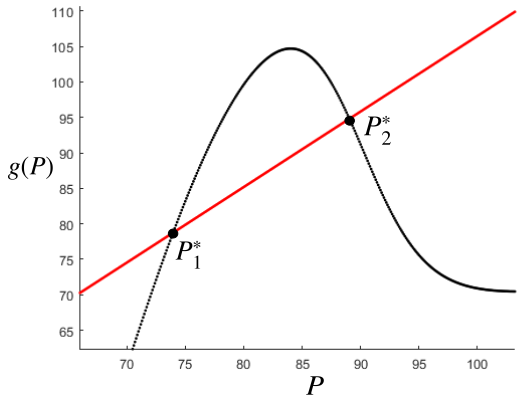

Figure 3: Graphical computation of the equilibrium points.

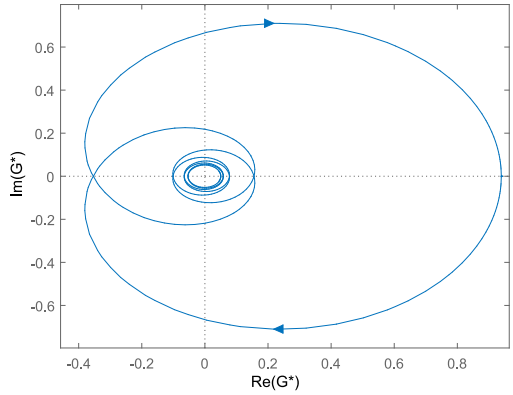

Figure 4: Nyquist diagram of $G^*(s)$ with $\tau = 1$.

shows the Nyquist diagram of $G^*(i\omega)$ with $\tau = 1$. From (6), the curve starts with $\omega = 0$ at point $a(r+R) = 0.9392$. Then, it is only necessary to analyze the equilibrium point P_2^*. The equilibrium point P_1^* is unstable as $1/J_1 = 0.2278 < a(r+R) = 0.9392$, thus the critical point is surrounded by the curve independently of the value of τ.

For P_2^*, the critical stability condition is

$$G^*(i\omega_0) = \frac{a\,[w_t(r+R) + ir\omega_0]}{w_t + i\omega_0} e^{-i\omega_0\tau} = \frac{1}{J_2}, \tag{10}$$

and it follows that

$$\left\{ \begin{array}{rcl} J_2 a w_t (r+R) & = & w_t \cos(\omega_0\tau) - \omega_0 \sin(\omega_0\tau), \\ J_2 a r \omega_0 & = & \omega_0 \cos(\omega_0\tau) + w_t \sin(\omega_0\tau). \end{array} \right. \tag{11}$$

From the above equations, one has

$$(J_2 a)^2 \left[w_t^2 (r+R)^2 + r^2 \omega_0^2 \right] = w_t^2 + \omega_0^2,$$

and the critical Hopf frequency can be computed as

$$\omega_0 = \sqrt{\frac{w_t^2\,[(J_2 a)^2 (r+R)^2 - 1]}{1 - (J_2 a)^2 r^2}} = 2.7602. \tag{12}$$

On the other hand, from (10) and considering the phase of each factor, one obtains

$$\arctan\left(\frac{r\omega_0}{w_t(r+R)}\right) - \arctan\left(\frac{\omega_0}{w_t}\right) - \omega_0\tau = \pi + 2m\pi, \;\; m \in \mathbb{Z}, \tag{13}$$

and the critical delay values which provokes the Hopf bifurcation is

$$\begin{array}{rcl} \tau_0 & = & \dfrac{1}{\omega_0}\left[\arctan\left(\dfrac{r\omega_0}{w_t(r+R)}\right) - \arctan\left(\dfrac{\omega_0}{w_t}\right) - \pi + 2\pi\right] \\ & = & 0.7248, \end{array} \tag{14}$$

which was obtained assigning $m = -1$ in (13), to make the term in brackets positive. Notice that the above critical delay value differs from the one reported in [2], where the authors found it to be between 0.6 and 0.7 s.

To construct approximations of the emerging periodic solutions, the graphical Hopf bifurcation theorem (GHBT) is used [7, 9]. The goal is to solve graphically the following equation for θ and ω:

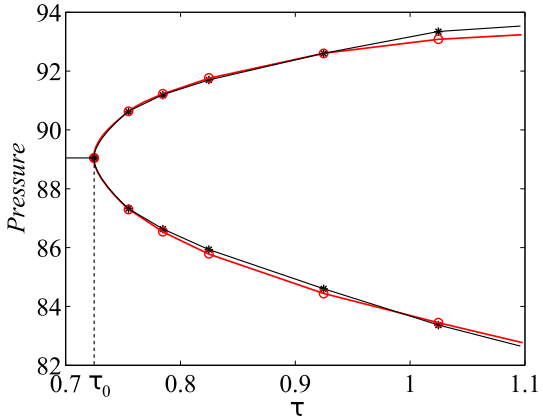

Figure 5: Amplitudes (maxima and minima) of oscillations obtained via numerical simulations (in red) and the corresponding approximations via GHBT (in black).

$$G^*(i\omega)J_2 = 1 + \xi(\tilde{\omega})\theta^2, \tag{15}$$

which is equivalent to find the intersection between the locus of $G^*(i\omega)J_2$ and the vector $1 + \xi(\tilde{\omega})\theta^2$. In the above equation, ξ is a complex number depending on the higher-order derivatives of $g(P)$, θ represents the amplitude of the periodic solution, ω is its frequency, and $\tilde{\omega}$ is an approximate frequency used to compute ξ, which here is simply taken as ω_0. The approximate periodic solution is recovered as

$$P(t) \approx P_2^* + \mathrm{Re}\left\{ \sum_{k=0}^{2} Y^k e^{i\omega k t} \right\}, \tag{16}$$

where $Y^0 = \theta^2 V_0$, $Y^1 = \theta$, $Y^2 = \theta^2 V_2$, and

$$V_0 = \frac{1}{4} H(0) \frac{d^2 g}{dP^2}\Big|_{P_2^*} \quad V_2 = \frac{1}{4} H(i2\omega) \frac{d^2 g}{dP^2}\Big|_{P_2^*},$$

with $H(s)$ given by (9) with $k = 2$. Using the above expressions, the complex ξ in (15) is computed as

$$\xi = -G^*(i\omega)\left[\frac{d^2 g}{dP^2}\Big|_{P_2^*}(V_0 + V_2) + \frac{1}{8}\frac{d^3 g}{dP^3}\Big|_{P_2^*} \right].$$

By solving (15) graphically and computing (16) for several values of the bifurcation parameter τ, one can obtain the plot of Fig 5. It shows the amplitudes (maxima and minima) of the periodic solutions existing for $\tau > \tau_0$. The results obtained using the GHBT are shown in black and the results of numerical simulations are shown in red, for comparison purposes.

3.1. Variation of the peripheral resistance

Consider now a variation of the peripheral resistance R. As can be seen from (7) and Fig. 3, when R decreases, the equilibrium point P_2 moves to lower values, and when R increases, P_2 moves to higher values. Moreover, there is a critical value, $R_{crit} \approx 1006.239$, for which the two equilibrium points collide, and they disappear for $R < R_{crit}$. That is, there is a saddle-node of equilibrium points for

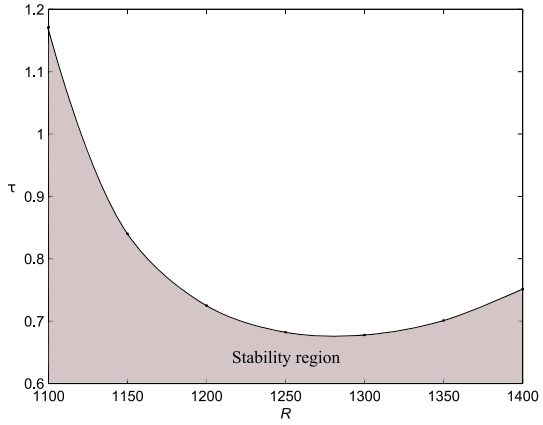

Figure 6: Stability region on the $R - \tau$ plane.

$R = R_{crit}$. This phenomenon can be interpreted graphically from Fig. 3. As R diminishes, the slope of the straight line increases, and the two equilibrium points become closer, until for $R < R_{crit}$, there are no equilibrium points. This condition can also be deduced from (11) setting $\omega_0 = 0$, which gives $J_2\, a\, w_t(r + R) = w_t$, i.e.,

$$g'(P_2) = \frac{1}{a(r + R)},$$

that is, the slope of $g(P)$ at P_2 equals the slope of the straight line. However, this bifurcation occurs for a value of R which is far from the nominal value reported for healthy individuals.

Figure 6 shows the stability region on the $R - \tau$ parameter plane, bounded by a Hopf bifurcation curve. It was obtained by varying R, and finding the critical τ value from (11). Moreover, the curvature coefficient, given by

$$\sigma_0 = \mathrm{Re}\left\{\frac{\xi}{dG^*(s)/ds|_{s=i\omega_0}\ J_2}\right\}, \qquad (17)$$

has been computed all along the Hopf curve. It indicates that, the whole curve represents supercritical Hopf bifurcations, i.e., they provoke the appearance of stable limit-cycles. Equation (17) shows a simplified form of σ_0 for SISO (single input - single output) systems. The general expression can be found in [6, 7].

3.2. Variation of the arterial compliance

Consider a variation of the capacity C, the arterial compliance, which models the elasticity and extensibility of the major artery. The value of the equilibrium point P_2 does not depend on C. Figure 7 shows the stability region on the $C - \tau$ parameter plane, delimited by a Hopf bifurcation curve. It was obtained by varying C and determining the critical τ value from (11), which increases linearly with C. Again, as confirmed using (17), all the Hopf bifurcation points on the curve represent supercritical bifurcations, giving birth to stable periodic solutions.

According to the above results, individuals with less elasticity on the major artery are more prone to instability than those with more elasticity.

4. Conclusions

In this work, some novel results about Cavalcanti & Belardinelli's model [2] have been established. The existence of a saddle-node of equilibrium points and the determination of stability regions in two-parameter spaces, together with approximations of the periodic solutions, have been found analytically by exploiting the advantages of a frequency-domain approach.

5. Acknowledgements

This work was supported by UNRN (PI 40/A389), UNS (PGI 24/K064), ANPCyT (PICT 2014-2161) and CONICET (PIP 112-201201-00144).

References

[1] Cherry E. M., F. H. Fenton, T. Krogh-Madsen and S. Luther, "Introduction to focus issue: complex cardiac dynamics," *Chaos*, vol. 20, 093701(1-8), (2017).

[2] Cavalcanti S. and E. Belardinelli, "Modeling of cardiovascular variability using a differential delay equation," *IEEE Trans. on Biomedical Engineering*, vol. 43(10), pp.982–989 (1996).

[3] Ottesen J. T., "Modelling of the baroreflex-feedback mechanism with time-delay," *J. of Math.*, vol. 36, pp.41–63 (1997).

[4] Ataee P., J. Hahn, G. A. Dumont, H. A. Noubari and W. T. Boyce, "A model-based approach to stability analysis of autonomic-cardiac regulation," *Comp. in Biol. and Medicine*, vol. 61, 119-126 (2015).

[5] Codrean A. and T. L. Dragomir, "Delay effect on cardiovascular regulation - A systems analysis approach," *Proc. of the 2015 European Control Conference,* 2731-2737 (2015).

[6] Mees A. I. and L. O. Chua, "The Hopf bifurcation theorem and its applications to nonlinear oscillations in circuits and systems," *IEEE Trans. Circ. Syst.*, vol. 4, 235-254 (1979).

[7] Moiola J. L. and G. Chen, Hopf Bifurcation Analysis: A Frequency Domain Approach. World Scientific Publishing Co, Singapore (1996).

[8] Catanho M., M. Sinha and V. Vijayan, "Model of aortic blood flow using the Windkessel effect," *Mathematical Methods in Bioengineering*, BENG 221 Report (2012).

[9] Gentile F. S., J. L. Moiola and E. E. Paolini, "On the study of bifurcations in delay-differential equations: a frequency-domain approach," *Int. J. of Bif. and Chaos*, vol. 22(6), 1250137(1-15), (2012).

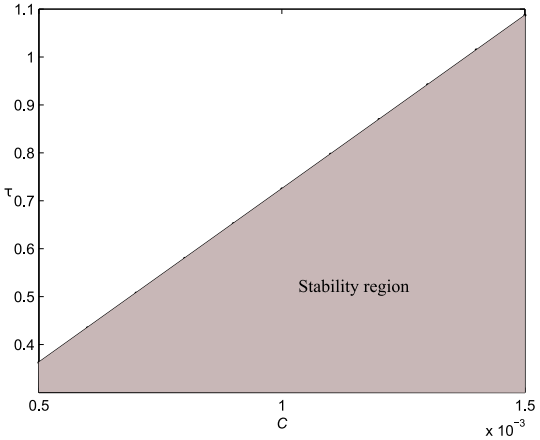

Figure 7: Stability region on the $C - \tau$ plane.